Molecular Dynamics Simulations of the Oxidation of Aluminum Nanoparticles

Saman Alavi,[†] John W. Mintmire,[‡] and Donald L. Thompson*[,†]

Department of Chemistry, University of Missouri−Columbia, Columbia, Missouri 65211 and Department of Physics, Oklahoma State University, Stillwater, Oklahoma 74078

Received: August 23, 2004; In Final Form: October 13, 2004

The oxidation of aluminum nanoparticles is studied with classical molecular dynamics and the Streitz−Mintmire (Streitz, F. H.; Mintmire, J. W. *Phys. Rev. B* **1994**, *50*, 11996) electrostatic plus (ES+) potential that allows for the variation of electrostatic charge on all atoms in the simulation. The structure and charge distributions of bulk crystalline α-Al_2O_3, a surface slab of α-Al_2O_3 with an exposed (0001) basal plane, and an isolated Al_2O_3 nanoparticle are studied. Constant NVT simulations of the oxidation of aluminum nanoparticles are also performed with different oxygen exposures. The calculations simulate a thermostated one-time exposure of an aluminum nanoparticle to different numbers of surface oxygen atoms. In the first set of oxidation studies, the overall approximate ratios of Al to O in the nanoparticle are 1:1 and 2:1. The nanoparticles are annealed to 3000 K and are then cooled to 500, 1000, or 1500 K. The atomic kinetic energy is scaled during the simulation to maintain the desired temperature. The structure and charge distributions in the oxidized nanoparticles differ from each other and from those of the bulk Al_2O_3 phases. In the Al_1O_1 simulation, an oxide shell forms that stabilizes the shape of the particle, and thus the original structure of the nanoparticle is approximately retained. In the case of $Al_1O_{0.5}$, there is insufficient oxygen to form a complete oxide shell, and the oxidation results in particles of irregular shapes and rough surfaces. The particle surface is rough, and the nanoparticle is deformed.

I. Introduction

Nanoparticles and their applications have attracted much attention in recent years.[1−3] Nanoparticles range from about 10 to 10^6 atoms with diameters from 1 to 100 nm. The size dependence of electron delocalization, band gaps,[4] specific heats,[5] and melting points[6] is characteristic of nanoparticles. Because of the high surface-to-volume ratios, undercoordinated surface atoms can be a significant fraction of the total number of atoms. This can cause significantly higher reactivity and large differences in other properties compared with those of the bulk material. Molecular dynamics simulations of nanoparticles of metallic and semiconductor materials require potential energy functions that account for the nonuniform charge distributions of the atoms in different parts of a nanoparticle. Ab initio molecular dynamics[7] does this but for large, nonperiodic systems is presently very time-consuming. A practical alternative is a variable-charge model, such as the electrostatic plus (ES+) potential of Streitz and Mintmire.[8,9] This potential, which is designed for metallic and ceramic materials, was parametrized for aluminum metal and aluminum oxide by Steitz and Mintmire[8] and applied to the calculation of surface and bulk properties of these materials and extended to parallel molecular dynamics simulations by Keffer and Mintmire.[9] The ES+ potential, with the addition of potential terms to account for the O_2 bond, has been used in simulations of aluminum nanoparticles with an unlimited supply of molecular oxygen,[10,11] The simulations[10,11] reproduced important features of Al oxidation, such as the thickness of the passivating oxide layer around the aluminum core.[12,13] We report here the results of MD simulations using the ES+ potential of the oxidation of aluminum nanoparticles following a one-time exposure to oxygen atoms. The purpose is to investigate the oxidation when the metal is exposed to a limited supply of oxygen, as when it is used as a solid rocket propellant. Special emphasis is placed on comparing the structure and charge distribution of the oxidized nanoparticles with bulk aluminum oxide.

The Streitz−Mintmire potential is briefly discussed in section II. The molecular dynamics simulations and the results are given in section III. A discussion follows in section IV, and the paper ends with a summary in section V.

II. Electrostatic Plus Potential

The electrostatic plus (ES+) potential of Streitz and Mintmire[8] is used in the molecular dynamics calculations. This potential treats electrostatic charges on aluminum and oxygen atoms in the simulation as variables. The total potential energy U_{pot} in the ES+ model is a function of the positions, $\{\mathbf{r}\}$, and charges, $\{q\}$, of the atoms and is composed of a long-range electrostatic contribution, U_{es}, and a short-range embedded-atom method (EAM) interaction U_{eam}:

$$U_{pot}(\{\mathbf{r}, q\}) = U_{es}(\{\mathbf{r}, q\}) + U_{eam}(\{\mathbf{r}\}) \quad (1)$$

The electrostatic contribution has an atomic electrostatic energy component for all N atoms in the system and contributions from Coulombic pair interactions V_{ij}:

$$U_{es}(\{\mathbf{r}, q\}) = \sum_{i=1}^{N}(\chi_i^0 q_i + J_i^0 q_i^2) + \frac{1}{2}\sum_{i\neq j} V_{ij}(\mathbf{r}_{ij}; q_i, q_i) \quad (2)$$

where χ_i^0 is the electronegativity and J_i^0 the hardness of atom i. The electronic charge density, $\rho_{i,}$ is the sum of an *effective*

* Corresponding author. E-mail: thompsondon@missouri.edu.
† University of Missouri−Columbia.
‡ Oklahoma State University.

10.1021/jp046196x CCC: $30.25
Published on Web 12/02/2004

nuclear charge, Z_i, and a valence electron charge distribution f_i:

$$\rho_i(\mathbf{r}; q_i) = Z_i\delta(\mathbf{r} - \mathbf{r}_i) + (q_i - Z_i)f_i(|\mathbf{r} - \mathbf{r}_i|) \quad (3)$$

In the present calculations, the valence electron charge distribution about an atomic nucleus is taken to have the form of a Slater-type 1S orbital,

$$f_i(r) = \left(\frac{\zeta_i^3}{\pi}\right)\exp(-2\zeta_i r) \quad (4)$$

where ζ is the decay length of the orbital. The Coulombic pair interactions are obtained from charge densities about each of the atomic nuclei,

$$V_{ij}(r_{ij}; q_i, q_j) = \int\int d\mathbf{r}_1\, d\mathbf{r}_2 \frac{\rho_i(\mathbf{r}_1; q_i)\, \rho_j(\mathbf{r}_2; q_j)}{r_{12}} \quad (5)$$

The evaluation of the two-center Coulomb integrals that arise from substituting eqs 3 and 4 into eq 5 is standard.[14] The variable atomic charges, $\{q\}$, in the potential are determined by minimizing the electrostatic energy subject to the constraint of zero net charge (i.e., $\sum_{i=1}^{N} q_i = 0$).

The embedded-atom contribution to the potential in eq 1 is given as a sum of the attractive embedding energy, F_i, and a repulsive residual pair interaction, ϕ_{ij},

$$U_{\text{eam}}(\{\mathbf{r}\}) = -\sum_{i=1}^{N} F_i[P_i] + \sum_{i<j}\phi_{ij}(r_{ij}) \quad (6)$$

The Finnis−Sinclair[15] functional dependence on the local electron density, P_i, is used to obtain the embedding energy,

$$F_i[P_i] = -A_i\sqrt{\frac{P_i}{\xi_i}} \quad (7)$$

where A_i is a positive constant. The local electron density of atom i is the sum of the electron densities from all of the other atoms,

$$P_i(r_i) = \sum_{i\neq j}\xi_j \exp[-\beta_{ij}(r_{ij} - r_{ij}^*)] \quad (8)$$

The repulsive residual pair interactions of eq 6 are

$$\phi_{ij}(r) = 2B_{ij}\exp\left[-\beta_{ij}\left(\frac{r - r_{ij}^*}{2}\right)\right] - C_{ij}[1 + \alpha_{ij}(r - r_{ij}^*)]\exp[-\alpha_{ij}(r - r_{ij}^*)] \quad (9)$$

The constants A_i, ξ_i, β_{ij}, α_{ij}, r_{ij}^*, B_{ij}, and C_{ij} for Al and O atoms and also for the Al−Al, O−O, and Al−O pair interactions were determined by fitting the predicted cohesive energies, lattice parameters, elastic constants of aluminum metal and alumina, and the surface energies of several low-index faces to experimental values. The atomic and pair parameters used in the potential energy function are given in Table 1. Further details are given in refs 8 and 9.

III. Molecular Dynamics Calculations and Results

Molecular dynamics simulations on nanoparticles were performed for the NVT ensemble. The equations of motion were integrated using the leapfrog algorithm[16,17] with a time step of 2 fs. In nanoparticle simulations, long-range electrostatic forces between the atoms were calculated directly, whereas the forces in the simulations of bulk phases were evaluated using Ewald summation techniques.[16] Cubic initial configurations were chosen for the nanoparticle simulations. These structures were annealed and equilibrated by starting the simulations at 3000 K and gradually cooling to the desired temperature within 1000 time steps. The temperature was scaled during the annealing process every 10 time steps by velocity scaling. After annealing, data were accumulated over 40 ps (unless otherwise stated) at the temperature of interest to calculate time averages.

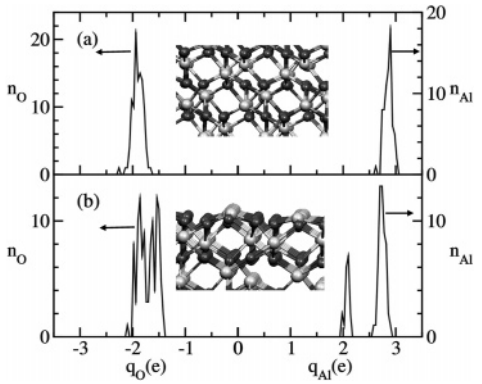

Figure 1. (a) Charge distribution for oxygen and aluminum atoms, n_O and n_{Al}, in bulk α-Al_2O_3 at 500 K as a function of the charges q_O and q_{Al} in units of electron charge. The charges on the oxygen atoms are narrowly distributed around −2, and those on the aluminum atoms are distributed around +3. A portion of the solid-state structure is given to show the equivalent oxygen and aluminum atoms. (b) Charge distribution on a slab of α-Al_2O_3 of finite thickness with an exposed (1000) basal plane at 300 K. The different charge distribution for the surface-layer oxygen and aluminum atoms is evident. The surface atoms are undercoordinated with respect to those in the bulk.

To provide reference values for atomic charges and density in the nanoparticle simulations, we performed molecular dynamics calculations with the ES+ potential on bulk aluminum oxide and the relaxed α-Al_2O_3(0001) basal plane at 500 K. A time step of 1 fs and a total time of 5 ps were used for these simulations. The initial input geometry of the ions in these calculations was the experimental equilibrium bulk geometry; therefore, shorter overall simulation times were required.

The electrostatic charge distributions for aluminum and oxygen for bulk α-Al_2O_3 and a relaxed α-Al_2O_3 (1000) surface slab at 500 K are shown in Figure 1a and b, respectively. In the bulk α-Al_2O_3 structure, aluminum and oxygen atoms have coordination numbers of 6 and 4, respectively. In this case, as seen in Figure 1a, the ES+ potential gives narrowly distributed charges of +3 and −2 for Al and O atoms, respectively. The surface Al and O atoms in Figure 1b have reduced coordination numbers of 4 and 3, respectively, and carry smaller absolute charges. The bimodal distribution of charge is seen in both Al and O atoms. The surface atoms carry smaller charges, whereas those inside the slab have charges similar to bulk values.

Molecular dynamics simulations were performed on a nanoparticle of Al_2O_3 with a total of 986 atoms. The final structure of the nanoparticle after annealing to 3000 K followed by equilibration for 40 ps at 500 K is shown in Figure 2a. This structure has an approximate diameter of 30 Å, with mostly oxygen atoms exposed on the surface of the nanoparticle. The density of the nanoparticle averaged over a radius of 12 Å from the center of mass is 3.296 g/cm^3, approximately 10% less than the bulk value. The room-temperature density of bulk aluminum oxide is 3.965 g/cm^3, and the melting point of the bulk phase at atmospheric pressure is 2345 K.[18] The charge distributions in this nanoparticle are given in Figure 2b. The charge

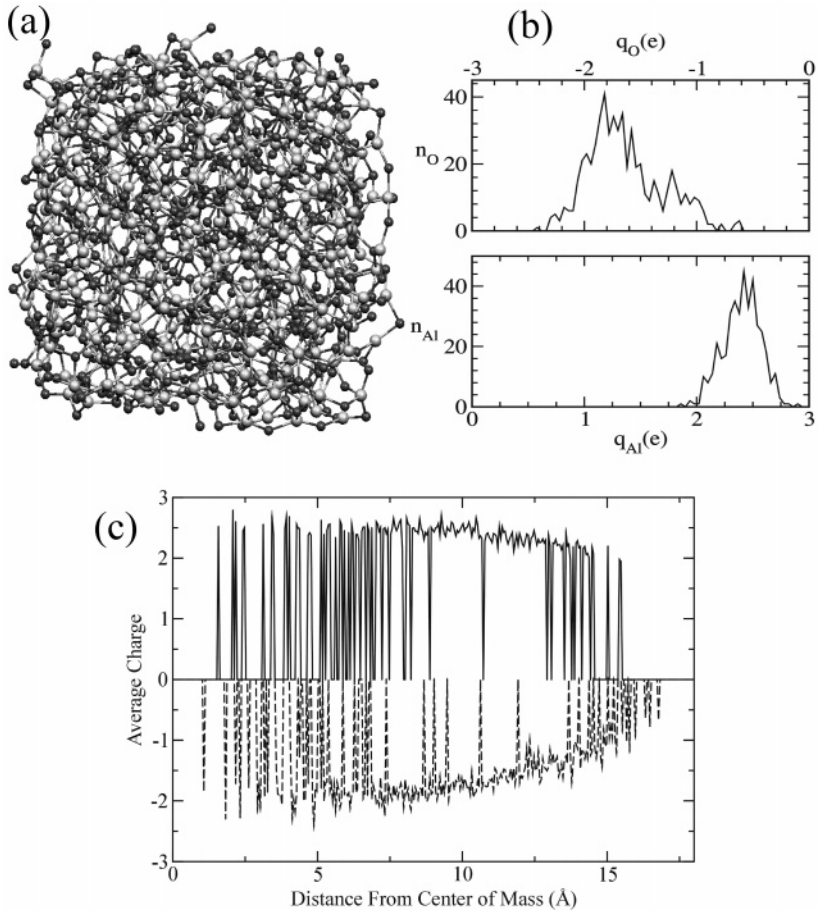

Figure 2. (a) Structure of an Al_2O_3 nanoparticle with 592 oxygen and 394 aluminum atoms at 500 K after a time of 40 ps following annealing at 3000 K. (b) Charge distribution for oxygen and aluminum atoms, n_O and n_{Al}, of the nanoparticle as a function of the charge q (in units of electron charge). (c) Charge distribution for the Al and O atoms as a function of the distance from the nanoparticle center of mass. The magnitudes of the charges decrease with increasing distance from the center of the nanoparticle.

distributions on the atoms are broader than those of bulk α-alumina. The sharp distinctions seen in Figure 1b between the charges of the surface and bulk atoms are blurred in the nanoparticle. The different charge densities on the nanoparticle surface compared to those on the bulk surface can lead to surface reactivities that are significantly different in the two phases.

Greater details of the charge distribution within the nanoparticle are given in Figure 2c, which shows the average charges of the Al and O atoms as functions of distances from the center of mass of the nanoparticle. From the center of the nanoparticle to a radius of ∼10 Å, the charges on the Al atoms are between $+3e$ and $+2.5e$ and those on the O atoms are $\sim -2e$. As the distance extends to the surface of the nanoparticle (radii greater than 10 Å from the center), the atoms become undercoordinated, and the absolute values of the charges on the Al and O atoms begin to drop. The O atoms are exposed on the surface to a greater extent than Al, and as a result, they are more undercoordinated and have smaller absolute values of charge ($<1e$) at the surface.

A calculation was performed on a $5 \times 5 \times 5$ face-centered cubic (fcc) nanoparticle of aluminum atoms at 500 K. The experimental melting point of bulk aluminum is 933.5 K,[18] so this simulation temperature corresponds to the solid phase. A snapshot of the resulting structure of the nanoparticle is shown in Figure 3a. The initial cubic shape of the nanoparticle has relaxed to a randomized spherical shape by the annealing and equilibration cycle. The average density of the nanoparticle up to a radius of 12 Å from the center of mass is 2.60 g/cm^3. The experimental density of bulk solid aluminum at 300 K is 2.70

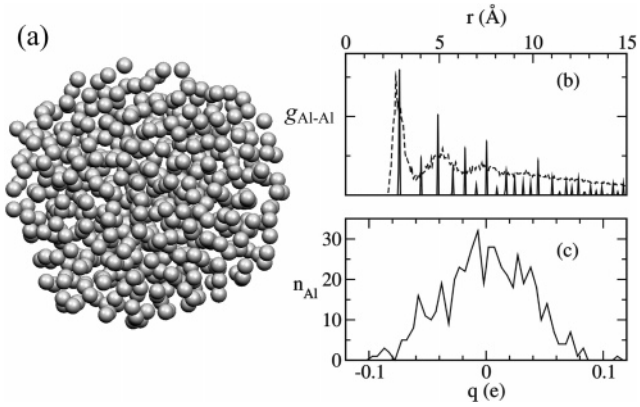

Figure 3. (a) Snapshot of the structure of a pure aluminum nanoparticle at 500 K. The nanoparticle consists of 500 aluminum atoms and was annealed to 3000 K before being cooled to the final temperature. (b) Radial distribution function, $g_{Al-Al}(r)$ for the aluminum nanoparticle (- - -) and bulk crystalline aluminum (−). (c) Charge distribution from the Streitz−Mintmire potential for the aluminum nanoparticle. The absolute values of the charge on the atoms are small.

g/cm^3.[18] The aluminum−aluminum radial distribution function (RDF), $g_{Al-Al}(r)$, is defined as

$$g_{Al-Al}(r) = \frac{1}{nN}\left\langle \sum_i \sum_j \delta[r - r_{ij}] \right\rangle \qquad (10)$$

where N is the total number of aluminum atoms, n is the number density, and r_{ij} is the separation between aluminum atoms i and

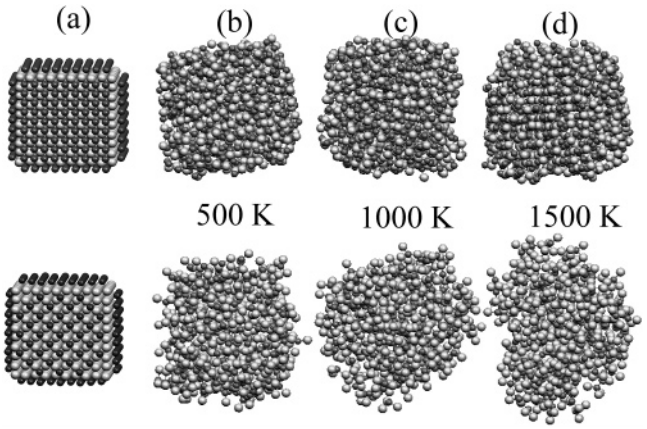

Figure 4. (a) Initial configurations for the 1:1 (top row) and 2:1 (bottom row) Al/O oxidation calculations. These structures are annealed to 3000 K before being equilibrated to the final temperatures. Snapshots at 40 ps of the nanoparticle calculations at (b) 500, (c) 1000, and (d) 1500 K. The top row shows the structures of the 1:1 nanoparticles, and the bottom row shows the structures of the 2:1 nanoparticles. The 2:1 nanoparticles have a tendency to fragment.

j. The RDF of the aluminum atoms in the nanoparticle is given in Figure 1b along with the original RDF of the aluminum atoms of the face-centered cubic supercell. The short-range, nearest-neighbor shell structures are retained in the nanoparticle, but long-range order is lost. Despite the amorphous structure and the undercoordination of the surface aluminum atoms, the charge distribution on the atoms in this nanoparticle, shown in Figure 1c, remains narrowly centered on zero, the value from bulk aluminum. Undercoordination of the surface Al atoms in this metallic nanoparticle does not cause a local accumulation of charge.

Simulations of the oxidation of aluminum nanoparticles were performed on a $5 \times 5 \times 5$ face-centered cubic supercell with 500 aluminum atoms. To mimic oxidation by surface oxidants, oxygen atoms are placed adjacent to the aluminum atoms on the faces of the supercell. The nanoparticles were then annealed to 3000 K before being equilibrated to final temperatures of 500, 1000, or 1500 K. The use of atomic rather than molecular oxygen simulates interactions with oxidizers such as nitramine and nitro compounds that deposit atomic oxygen on the aluminum surface.[20]

Calculations were performed with different ratios of aluminum to oxygen. The configuration in the top row of Figure 4a shows the initial state of the nanoparticles with approximate 1:1 and 2:1 ratios of Al to O. In the first case, the faces of the aluminum cube are covered by oxygen atoms at the beginning of the simulation, and the mole ratio of the nanoparticle is $Al_1O_{0.97}$. This simulates conditions where a large supply of oxidizer is initially available to the aluminum, but the supply is not replenished. The second set of calculations (bottom row in Figure 4a) were done with less than half of the area of each face covered with oxygen atoms and an atomic ratio of $Al_1O_{0.44}$. For both sets of oxygen exposure, calculations were performed at 500, 1000, and 1500 K. The nanoparticles were annealed to 3000 K and cooled prior to equilibration. A time step of 2 fs was used, and the total time of the calculations was 40 ps after annealing. Snapshots of the nanoparticles at 40 ps are shown in Figure 4b−d. For the 1:1 nanoparticle, the general shape is retained, and the surface remains relatively smooth. The surfaces of the nanoparticles for the oxygen-deficient 2:1 case show a tendency to roughen, and the shape of the nanoparticles changes significantly. In the Al/O 1:1 ratio, the aluminum oxide layer forms a complete coating around the aluminum core. This coating prevents the roughening of the nanoparticle surface structure and the break up of the structure. It should be noted that the excess heat generated by the reaction of the oxygen and aluminum atoms is removed by the temperature scaling; therefore, the surface roughening is not related to the heat of reaction. Furthermore, heat generated from the reaction would affect the 1:1 nanoparticle to a greater extent because there are more oxygen atoms available for reaction.

The charge distributions for Al/O ratios of 2:1 and 1:1 nanoparticles at 500 K are given in Figure 5a and b, respectively. The aluminum atoms have smaller absolute charges in the oxygen-deficient 2:1 nanoparticle compared to those in the 1:1 or Al_2O_3 nanoparticles. In both cases, the charge distributions are broader, and the charges are shifted to lower values than those of bulk α-alumina and the surface slab. In both the 2:1 and 1:1 nanoparticles, the oxygen atoms are saturated and have charges close to $-2e$. The average charges of the Al and O atoms as functions of the distance from the centers of mass of the 2:1 and 1:1 nanoparticles are shown in Figure 5c and d, respectively. The absolute values of the charges are smaller in the 2:1 nanoparticle.

Figure 6 shows a comparison between the radial distribution functions for the 2:1 (dashed lines) and 1:1 (solid lines) nanoparticles at 40 ps. Although the overall structures of the nanoparticles are different, the nature of the short-range bonding illustrated by the RDFs is similar.

Although individual Al−O bonds attain stable configurations for short times, the distribution of oxygen atoms with respect to the center of mass of the nanoparticle changes with time. Figure 7 shows the distribution of the oxygen atoms with respect to the center of mass of the 1:1 nanoparticle at three times during the simulation. The annealing process initiates the diffusion of the oxygen ions from the surface toward the interior of the nanoparticle. At 1 ps after annealing, the oxygen ions are in a band near the surface with no oxygen atoms penetrating deeply into the aluminum core of the nanoparticle. As time progresses, the atoms diffuse inward, and at the end of the simulation, the oxide forms a broad layer. However, at the end of the simulation, oxygen ions are still not uniformly distributed throughout the nanoparticle. This observation is in agreement with the behavior of aluminum in contact with oxygen, where the oxide forms a passivating coating on the solid aluminum.[12] Figure 7 shows that the distribution of oxygen atoms within the nanoparticle does not change appreciably between 20 and 40 ps after the annealing process. This indicates that the simulation time is sufficient on the basis of the diffusion of the oxygen atoms toward the core of the nanoparticles.

IV. Discussion

The $5 \times 5 \times 5$ fcc nanoparticle of pure aluminum at 500 K was simulated with annealing parameters similar to those used for the aluminum oxide nanoparticles. Within the 40-ps time of the simulation, the structure of the pure aluminum nanoparticle relaxes to a nearly spherical shape, and the charge distribution on the aluminum atoms in this nanoparticle is very narrow and centered about zero. The largest absolute value of the charge is $\sim 0.1e$. Appreciable charge transfer between the Al atoms in the nanoparticle does not occur, and the reactivity of the nanoparticle Al atoms will likely not be different from that of the bulk metal surfaces. The Al_2O_3 nanoparticle, however, is expected to react differently from the bulk. At 500 K, the nanoparticle retains some resemblance to its initial cubic shape after annealing and 40 ps of time evolution. The chemical bonds in covalent Al_2O_3 are stronger than in a pure aluminum nanoparticle, and a longer time scale would be required to relax

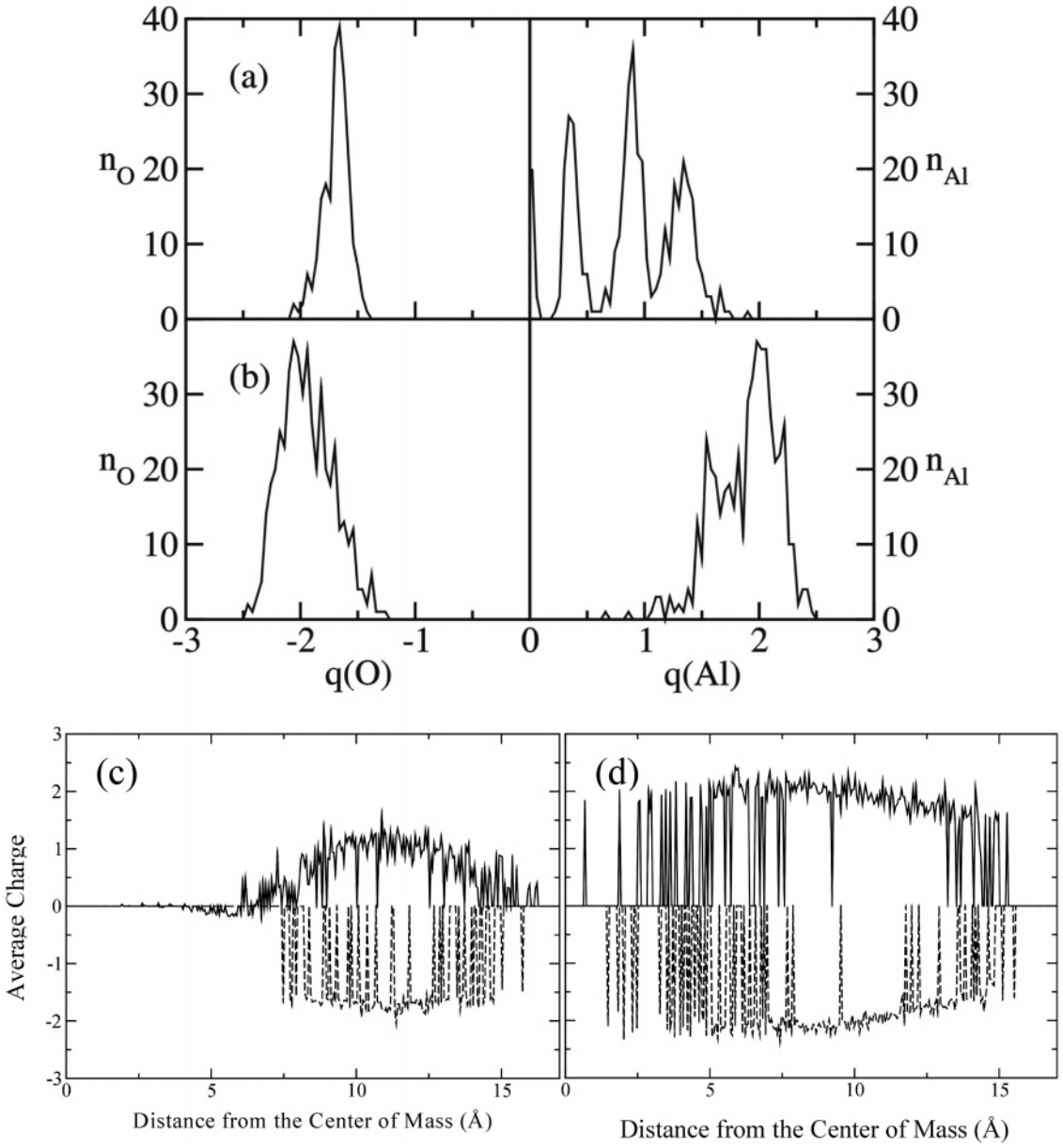

Figure 5. Charge distributions (in units of electronic charge) for (a) the 2:1 and (b) the 1:1 nanoparticles at 500 K. The charge distributions are broader than those of Figure 2, and the undersaturated aluminum atoms have lower charges. The average charges on the atoms in these two nanoparticles as functions of distance from the centers of mass are given in c for the 2:1 nanoparticle and in d for the 1:1 nanoparticle.

the nanoparticle to a stable, presumably spherical shape. The charge distribution is also very different from that of the bulk phases.

In studying oxidation, we observe that aluminum nanoparticles with complete oxide shells, such as in the case where the Al/O ratio is approximately 1:1, retain much of their initial structure after annealing and further time evolution, despite the fact that for the 1000 and 1500 K simulations the Al core should be melted. The amorphous oxide layer acts as a stabilizing shell for the aluminum core. In cases where a complete oxide layer cannot be formed, such as in the 2:1 nanoparticle, the nanoparticle deforms. This is observed in the simulation results for 500, 1000, and 1500 K shown in the bottom row of Figure 4.

Fragmentation and explosive behaviors of aluminum nanoparticles have been observed experimentally.[21] The fragmentation of the nanoparticle in oxygen-deficient environments observed in this work can have practical applications where Al is exposed to an oxidizer. If there is an excess of oxygen initially available such that the surface of the particles is saturated, then a stable oxide coating will form a passivation layer, which can effectively eliminate access to the Al atoms in the core. However, if aluminum nanoparticles are exposed to relatively small amounts of oxygen or the oxygen exposure occurs over a long time compared to the time scale of Al−O reactions, then the nanoparticles may fragment, which will expose more unreacted aluminum to the oxidizer.

The charge distributions of the aluminum and oxygen atoms in the aluminum oxide bulk and surface slabs are different from those of the nanoparticles. This can lead to different surface reactivities of the aluminum oxide nanoparticles and bulk phases with respect to adsorbate species. The aluminum and oxygen atoms on the nanoparticle surfaces are undercoordinated compared to those of a bulk surface. This can enhance their reactivity as Lewis acids and bases but can weaken the strength of electrostatic interactions on the nanoparticle oxide surface. The amorphous structure of the nanoparticle can also affect the rates of surface diffusion of adsorbates on the nanoparticle and therefore can affect the rate of surface reactions.

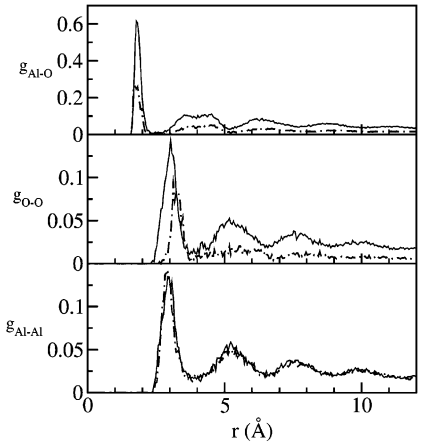

Figure 6. Al−O, O−O, and Al−Al radial distribution functions for a 1:1 nanoparticle at 500 K after annealing to 1500 K (-·-) and 40 ps later (−). The locations of the maxima and shapes of the curves do not change appreciably with time. This indicates that at the level of the chemical bond the annealing process has brought the atoms to a stable configuration.

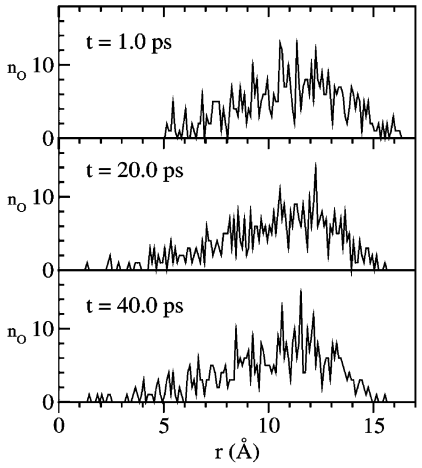

Figure 7. Distribution of oxygen atoms at 1, 20, and 40 ps as a function of the distance from the center of mass of a 1:1 nanoparticle annealed at 500 K. There is no large-scale diffusive motion of the oxygen atoms after 20 ps.

These studies show that there can be significant differences in the chemical reactivity of a nanoparticle and a bulk aluminum oxide surface. In nanoparticles of nonconducting materials, however, charge distribution among the atoms will be mostly determined by the internal molecular structure, with polarization from neighboring molecules playing a secondary role. These polarization effects can differ from bulk phases to nanoparticles, so a difference in reactivity may be seen in molecular materials as well.

Another difference in the reactivities of the nanoparticles is observed by comparing the surfaces of the stoichiometric Al_2O_3 and O-deficient nanoparticles (Figure 4). The surface of the Al_2O_3 nanoparticle is composed mostly of oxygen atoms, whereas the surfaces of the other nanoparticles are mostly aluminum atoms. The Al atoms relax into the surface in the stoichiometric 2:3 nanoparticle to expose mostly the oxygen atoms on the surface. This could indicate some flexibility in the design of the aluminum oxide nanoparticles suitable for specific applications; for example, nanoparticles with predominantly exposed Al or O sites on the surface might be designed for the catalysis of a particular type of reaction or for preferential adsorption of a particular species.

V. Summary and Conclusions

The structures of aluminum oxide bulk phases and nanoparticles have been studied with NVT molecular dynamics, and comparisons have been made between the structures and charge distributions in the different cases. The charge distribution in the nanoparticles is much broader than that in the periodic bulk solid. The dynamics of the oxidization of a pure aluminum nanoparticle in contact with different amounts of oxygen are also studied. The nature of individual chemical bonds (particularly Al−O bonds) in nanoparticles with different oxygen contents is identical, but in low exposures where the oxide layer does not form a complete coating around the aluminum core, a tendency toward fragmentation is seen. Charge distributions among atoms in nanoparticles with varying amounts of oxygen can also be appreciably different.

Acknowledgment. This work was partially supported by the U.S. Army Research Office under grant number DAAD19-01-1-0503. J.W.M. acknowledges support from the U.S. Office of Naval Research.

References and Notes

(1) Gleiter, H. *Prog. Mater. Sci.* **1989**, *33*, 223.
(2) Gleiter, H. In *Mechanical Properties and Deformation Behaviour of Materials Having Ultrafine Microparticles*; Nastasi, M., Parkin, D. M., Gleiter, H., Eds.; Kluwer: Dordrecht, The Netherlands, 1993; p 30.
(3) *Nanoscale Materials in Chemistry*; Klabunde, K. J., Ed.; Wiley-Interscience: New York, 2001.
(4) *Physics and Chemistry of Metal Cluster Compounds*; de Jongh, J., Ed.; Kluwer: Dordrecht, The Netherlands, 1994.
(5) Bai, H. Y.; Luo, J. L.; Jin, D.; Sun, J. R. *J. Appl. Phys.* **1996**, *79*, 361.
(6) Shi, F. G. *J. Mater. Res.* **1994**, *9*, 1307.
(7) Car, R.; Parrinello, M. *Phys. Rev. Lett.* **1983**, *55*, 2471.
(8) Streitz, F. H.; Mintmire, J. W. *Phys. Rev. B* **1994**, *50*, 11996.
(9) Keffer, D. J.; Mintmire, J. W. *Int. J. Quantum Chem.* **2000**, *80*, 733.
(10) Campbell, T.; Kalia, R. J.; Nakano, A.; Vashishta, P.; Ogata, S.; Rodgers, S. *Phys. Rev. Lett.* **1999**, *82*, 4866.
(11) Kalia, R. K.; Campbell, T. J.; Chatterjee, A.; Nakano, A.; Vashishta, P.; Ogata, S. *Comput. Phys. Commun.* **2000**, *128*, 245.
(12) Sánchez-Lopéz, J. C.; González-Elipe, A. R.; Fernández, A. *J. Mater. Res.* **1998**, *13*, 703.
(13) Sato, S.; Ohshima, K.; Fujita, T. *J. Phys. Soc. Jpn.* **1990**, *59*, 662.
(14) Roothan, C. C. *J. Chem. Phys.* **1951**, *19*, 1445.
(15) Finnis, W.; Sinclair, J. E. *Philos. Mag. A* **1983**, *50*, 1285.
(16) Allen, M. P.; Tildesley, D. J. *Computer Simulation of Liquids*; Oxford University Pres: Oxford, England, 1987.
(17) Frenkel, D.; Smit, B. *Understanding Molecular Dynamics*, 2nd ed.; Academic Press: San Diego, 2002.
(18) *CRC Handbook of Chemistry and Physics*, 76th ed.; Lide, D. R., Ed.; CRC Press: Boca Raton, FL, 1995.
(19) Sorescu, D. C.; Boatz, J. M.; Thompson, D. L. *J. Phys. Chem. B* **2003**, *107*, 8953.
(20) Sayir, A. Unpublished work as quoted in ref 10.